A localized view on molecular dissociation via electron-ion partial covariance

Felix Allum,**,†,‡ Valerija Music,¶,§,∥ Ludger Inhester,*,⊥ Rebecca Boll,§ Benjamin Erk,∥ Philipp Schmidt,¶,§ Thomas M. Baumann,§ Günter Brenner,∥ Michael Burt,† Philipp Demekhin,¶ Simon Dörner,∥ Arno Ehresmann,¶ Andreas Galler,§ Patrik Grychtol,§ David Heathcote,† Denis Kargin,# Mats Larsson,@ Jason W. L. Lee,†,∥ Zheng Li,⊥,△ Bastian Manschwetus,∥ Lutz Marder,¶ Robert Mason,† Michael Meyer,§ Huda Otto,¶ Christopher Passow,∥ Rudolf Pietschnig,# Daniel Ramm,∥ Kaja Schubert,∥ Lucas Schwob,∥ Richard Thomas,@ Claire Vallance,† Igor Vidanović,# Clemens von Korff Schmising,♥ René Wagner,§ Peter Walter,†† Vitali Zhaunerchyk,‡‡ Daniel Rolles,¶¶ Sadia Bari,∥ Mark Brouard,† and Markus Ilchen*,∥,¶,§

† The Chemistry Research Laboratory, Department of Chemistry, University of Oxford, Oxford
OX1 3TA, United Kingdom

‡Stanford PULSE Institute, SLAC National Accelerator Laboratory, Menlo Park, CA, USA

¶Institut für Physik und CINSaT, Universität Kassel, Heinrich-Plett-Straße 40, D-34132 Kassel,

Germany

§European XFEL, Holzkoppel 4, 22869 Schenefeld, Germany

||Deutsches Elektronen-Synchrotron DESY, Notkestr. 85, 22607 Hamburg, Germany

\(\perp \) Center for Free-Electron Laser Science CFEL, Deutsches Elektronen-Synchrotron DESY,

Notkestr. 85, 22607 Hamburg, Germany

#Institut für Chemie, Universität Kassel, Heinrich-Plett-Straße 40, D-34132 Kassel, Germany

@Stockholm University, AlbaNova University Center, 114 21 Stockholm, Sweden

△State Key Laboratory for Mesoscopic Physics, School of Physics, Peking University, Beijing

100871, China

∇Max Born Institute, Max-Born-Straße 2A, 12489 Berlin, Germany
††SLAC National Accelerator Laboratory, 2575 Sand Hill Road, Menlo Park, California 94025,

USA

‡‡University of Gothenburg, 405 30 Gothenburg, Sweden

¶¶Kansas State University, 1228 N 17th St, KS 66506, United States of America

E-mail: fallum@stanford.edu; ludger.inhester@desy.de; markus.ilchen@desy.de

Abstract

Inner-shell photoelectron spectroscopy provides an element-specific probe of molecular structure, as core-electron binding energies are sensitive to the chemical environment. Short-wavelength femtosecond light sources, such as Free-Electron Lasers (FELs), even enable time-resolved site-specific investigations of molecular photochemistry. Here, we study the ultraviolet photodissociation of the prototypical chiral molecule 1-iodo-2-methylbutane, probed by XUV pulses from the Free-electron LASer in Hamburg (FLASH) through the ultrafast evolution of the iodine 4d binding energy. Methodologically, we employ electron-ion partial covariance imaging as a technique to isolate otherwise elusive features in a two-dimensional photoelectron spectrum arising from different photofragmentation pathways. The experimental and theoretical results for the time-resolved electron spectra of the $4d_{3/2}$ and $4d_{5/2}$ atomic and molecular levels that are disentangled by this method provide a key step towards studying structural and chemical changes from a specific spectator site.

1 Introduction

Molecular restructuring and its consequences for molecular function are of ubiquitous interest across a variety of scientific disciplines. The involved physical and chemical dynamics
typically progress on the femtosecond timescale, which can be observed in 'real-time' through
a range of ultrafast spectroscopic techniques. Modern technological developments in high
intensity short-wavelength FELs have extended such methods for probing ultrafast chemistry
in a site-selective manner by utilizing wavelengths of light which can selectively address core
orbitals. 2-9

Ultrafast molecular fragmentation can cause significant core-electron binding energy 9 changes. These changes are typically on the order of few eV for chemical shifts of neutral fragments, tens of eV for delocalized charges in the valence shell, and more than a hun-11 dred eV for localized core-holes. 10 Such shifts are measurable by photoelectron spectroscopy and can be used to study photochemistry in real-time from a specific observer site. 5-7 An often limiting factor of such studies is that it is difficult to distinguish smaller shifts from static signal originating from ground-state molecules and background. Additionally, relat-15 ing delay-dependent signal to a specific underlying process is challenging, particularly in 16 the case of more complex molecules which may undergo a range of photochemical processes following photoexcitation or -ionization. One potential solution to overcome this limita-18 tion is to utilize electron-ion correlations, allowing electron spectroscopy to be applied in 19 a channel-resolved manner, by isolating contributions in an electron spectrum correlated to a specific photofragmentation channel, determined by ion spectroscopy. 11-13 Electron-ion 21 coincidence techniques have proven to be very powerful, but are limited to very low count 22 rates, such that multiple particles produced in the same laser pulse can be assigned to a 23 single event. 14,15 While progress in coincidence experiments at FELs has been made, 2,9,16–18 sufficient data collection rates for highly differential insights into molecular fragmentation channels still poses a considerable technical challenge that can prospectively be tackled by high-repetition rate FELs. 19 Here, we exploit an alternative method to determine chargedparticle correlations at far higher count rates per photon pulse; through calculating the covariance, a measure of linear correlation between the signals of interest recorded over many data acquisition cycles (i.e. laser shots). ^{20–22} This holds the promise of being applicable even to larger molecules. ²³ Although the inherently unstable conditions due to stochastic pulse generation at Self-Amplified Spontaneous Emission (SASE) FELs provide challenges for correlation techniques, schemes have been developed to not only correct for the adverse effects of such fluctuations, but effectively exploit them through either partial ^{24,25} or contingent ²⁶ covariance analysis. In the present work, we demonstrate the extension of these techniques, usually applied to a 1D mass spectrum, to a 3D Velocity-Map Imaging (VMI) study of the ultrafast evolution of electronic structure during a photodissociation, at a particular core site, in a channel-resolved manner.

We use this technique in order to investigate properties and dynamics of the prototypical chiral molecule 1-iodo-2-methylbutane (C₂H₅CH (CH₃)CH₂I) at the iodine 4d edge, as it is a prominent candidate for approaching dynamical investigations of chirality with FELs in future studies. Understanding and benchmarking the underlying ultrafast photochemistry is an important prerequisite for these kind of studies. In particular, we UV-excite the molecule and predominantly trigger neutral dissociation at its carbon-iodine bond (shown schematically in Figure 1). We demonstrate the value of partial covariance analysis for following the iodine in its dynamical change from molecular to isolated atomic environments through channel-resolved photoelectron spectroscopy.

Results and Discussion

Samples of R/S-1-iodo-2-methylbutane were introduced as a continuous molecular beam, seeded in helium, into the CAMP end-station²⁷ at the beamline BL1 of FLASH 1²⁸ at DESY in Hamburg, Germany. The molecule was dissociated at its C-I bond following singlephoton UV excitation (267 nm (4.6 eV), \sim 150 fs, maximum pulse energy of 7 μ J). As is the case in alkyl iodides in general, ²⁹ photoabsorption in this region arises due to an excitation from the iodine lone pair (n_I) to the C-I antibonding ($\sigma*$) orbital. The evolving chemical dynamics following photoexcitation are investigated from the viewpoint of the released neutral iodine atom via a time-delayed, $\sim 63.5 \, \text{eV}$, FEL-based probe pulse with $\sim 50 \, \text{fs}$ duration and pulse energy at the target of about 1 μ J (see Methods section for details). Due to the large cross-section difference to other constituents and electronic orbitals, the I 4d orbital is predominantly ionized. ³⁰ The photoions and photoelectrons produced are velocity-mapped to a pair of position sensitive detectors ^{27,31–33} (as described in more detail in the Methods section). By using partial covariance analysis to select only electrons that are emitted from neutrally dissociated iodine, and following their time evolution during the photolysis, an

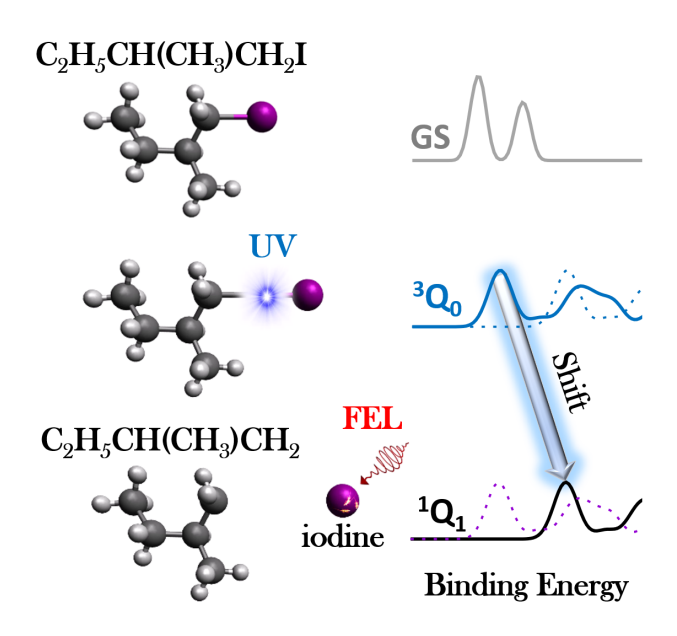


Figure 1: Schematic representation of the experimental scheme to study the ultrafast photodynamics of 1-iodo-2-methylbutane. Photoexcitation (predominantly to the excited state of 3Q_0 symmetry) is initiated by a UV pump pulse. The photoexcited molecule is interrogated at a series of pump-probe delays by a XUV-FEL pulse, probing the photoelectron binding energy of the I (4d) core orbital. Measured changes in the binding energy during the photodissociation can be related to the underlying photochemistry, supported by quantum simulations of the photoionization process. Illustration of the UV-induced fragmentation of 1-iodo-2-methylbutane, its subsequent dissociation along the C-I bond, and the iodine's underlying evolution from a molecular to an atomic environment.

- 63 advanced scheme for femtochemistry is enabled. The interpretation of the delay-dependent
- photoelectron spectra is supported by state-of-the-art simulations of photoionization.³⁴

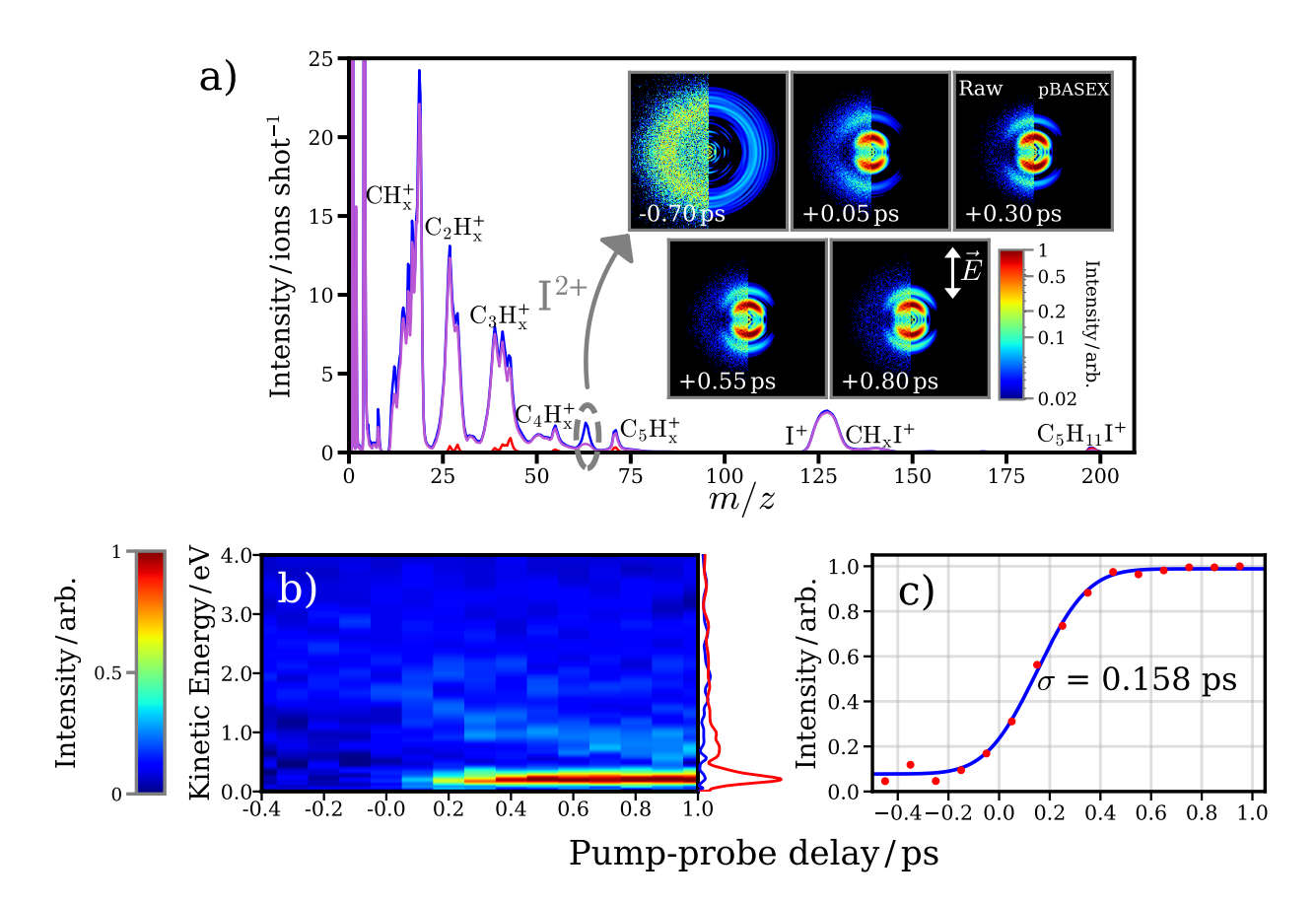


Figure 2: a) Normalized ion mass spectra recorded for 1-iodo-2-methylbutane with the XUV only (magenta), UV only (red) and UV early-XUV late at a pump-probe delay of +0.80 ps (blue). Inset: Raw (left) and reconstructed (right)³⁵ velocity-map I²⁺ ion images at a series of pump-probe delays. The -0.70 ps image's intensity has been multiplied by 5, to increase the visibility of the weak, high-KER channel. The polarization axis of the UV laser is vertical in these images. b) Delay-dependent kinetic energy distribution for the I²⁺ ion. The UV-early (>1 ps delay) and UV late (<-0.2 ps delay) distributions are projected in red and blue respectively. c) Integrated yield of the low kinetic energy (<0.4 eV) feature as a function of pump-probe delay (red points) with a fit to a normal cumulative distribution function (blue line).

⁶⁵ Velocity-map Ion Imaging

Figure 2a) shows mass spectra of 1-iodo-2-methylbutane exposed to the UV and XUV pulses alone, or with both pulses for positive pump-probe delays (UV preceding the XUV). At 67 the employed intensities, very little multi-photon dissociative ionization is initiated by the UV pulse alone, whereas the XUV pulse causes extensive ionic break-up. In the two-color experiment, a clear pump-probe signal can be observed most prominently in the I^{2+} ion, 70 whose yield is significantly enhanced when the UV pulse precedes the XUV. As ionization 71 at the I 4d orbital by the XUV predominantly results in two charges after Auger decay, ³⁰ 72 UV-induced neutral photodissociation followed by ionization at the nascent iodine atoms by 73 the XUV would lead to an enhanced I²⁺ signal at sufficiently large internuclear distances, for which charge transfer does not occur. 3 Small enhancements of other fragments are also 75 visible in comparison to the XUV-only spectrum. 76

Velocity-map images for the I²⁺ ion at a series of pump-probe delays, shown in the inset 77 of Figure 2a), provide insight into the UV-induced C-I dissociation. At negative pump-probe delays (UV late), a weak, broad feature at high radii is observed, that is assigned to a (multi-79 photon) XUV-induced Coulomb explosion of the parent molecule. When the UV pulse preexcites the molecules, two clear features emerge in the ion images. Firstly, there is a strong contribution at low radii, which is peaked along the UV polarization axis As is expected for one-photon transitions, intensity of this feature as a function of angle to the polarization axis, $I(\theta)$, is of the form $I(\theta) = (\sigma/4\pi)[1 + \beta P_2(\cos\theta)]$, where P_2 is the second Legendre polynomial, and β is the anisotropy parameter. This takes limiting values of -1 and +2 for transitions of pure perpendicular or parallel nature, respectively (under the assumption of a prompt photodissociation). 36,37 In the present case, a β value of ≈ 1.80 is extracted 87 $(\beta \approx 1.80^{-38})$. This is expected for neutral photodissociation following a parallel excitation predominantly to the ${}^{3}Q_{0}$ state, as observed in similar alkyl iodides. 29 The delay-dependent I²⁺ kinetic energy is plotted in Figure 2b), and panel c) shows the integrated intensity of the low kinetic energy, neutral dissociation feature. This signal rises on an ultrafast (few hundred

fs) timescale, as is expected for a direct dissociation, as observed previously in related alkyl iodides. ²⁹ The rise in intensity of this feature is somewhat delayed with respect to time-zero. This is to be expected as, at sufficiently early pump-probe delays, charge transfer can occur between the multiply charged iodide ion produced following XUV ionization and the recoiling C₄H₉ radical, reducing the low energy I²⁺ ions formed. Previous pump-probe studies using site-selective ionization in similar photodissociation molecules have examined differences in the delay-dependent behavior of multiple iodine charge states to extract information about distance-dependent charge-transfer probabilities. 3,4,8,39 However, in the present work, which employs a relatively weak XUV pulse which is only a few eV above the I 4d binding energy 100 of the neutral molecule, a range of iodine ion charge states are not populated, and thus the 101 extractable insights into charge transfer are limited and not discussed further in the present 102 manuscript. 103

Secondly, a weaker, more diffuse feature at higher radii is also visible after time-zero. 104 This moves towards the center of the image at longer pump-probe delays, indicative of a 105 Coulombic contribution to the fragment energy, which decreases at larger internuclear sepa-106 rations, i.e. longer pump-probe delays. 3,4,39 Covariance imaging analysis 39-42 confirms that 107 this minor channel arises from a multi-photon dissociative ionization by the pump pulse, prior to XUV absorption at the iodine site. At longer pump-probe delays, the double ionization at the iodine fragment occurs when the charged alkyl co-fragment is at a greater separation, and so the Coulombic contribution to the kinetic energy of this feature decreases 111 as pump-probe delay advances. This channel is not discussed further in the current work, 112 which focuses on the dominant, neutral photodissociation channel. As will be demonstrated 113 shortly, the electron-ion partial covariance imaging method used allows isolation of the pho-114 to electron signal correlated solely to the neutral dissociation feature of interest. As shown 115 in this section, the temporally and kinetic-energy resolved ion-yield evolution already pro-116 vides valuable information about the individual dissociation channels and allows to partially 117 disentangle them. Deeper insights about selective contributions and processes can then be 118

120 Electron-Ion Partial Covariance Imaging

The photodissociation dynamics can be further probed through time-resolved inner-shell 121 photoelectron spectroscopy 5-7,34 at the iodine 4d site, as demonstrated on the ultraviolet 122 photodissociation of methyl iodide by Brauße et al., in which a small increase in I 4d binding 123 energy was detected following UV excitation. This was assigned to ionization of dissociated 124 iodine atoms, supported by earlier synchrotron measurements of the I 4d binding energies 125 of CH₃I and I. ^{43–46} The ability to study the temporal evolution of the signal, however, 126 was hampered by the fact that this small contribution overlaps energetically with signal 127 arising from unpumped parent molecules (due in part to the significant FEL bandwidth); a limitation that can be tackled by the partial covariance analysis. A primary aspect of the current work is that this method can be utilized to isolate delay-dependent spectral features 130 of interest. 131

Photoelectron images following irradiation of 1-iodo-2-methylbutane (seeded in He) by 132 the UV and XUV lasers are plotted in Figure 3a). The strong rings observed in the helium-133 only case are due to single and double ionization of He by the XUV pulse, which form a 134 significant background when 1-iodo-2-methylbutane is present, labeled 'C₅H₁₁I' in Figure 135 3a). Subtraction of the helium-only background image, normalized by number of laser shots 136 and average FEL pulse energy yields Subtraction of background contributions yields the 137 image plotted on the right of panel a) of Figure 3. A feature at slightly lower kinetic 138 energy (higher binding energy) than the He²⁺ photoline is observed, arising from ionization 139 at the I 4d site in C₅H₁₁I. The associated electron binding energy spectrum (Figure 3c)) 140 shows two clear peaks at approximately 56.5 eV and 58.0 eV, which can be assigned to the 141 molecular $4d_{5/2}$ and $4d_{3/2}$ levels, respectively. In this simple association of electronic origins, 142 the energy difference is already a reliable parameter. A higher differential view on the angular distribution patterns is not only a valuable characterization of the given electron

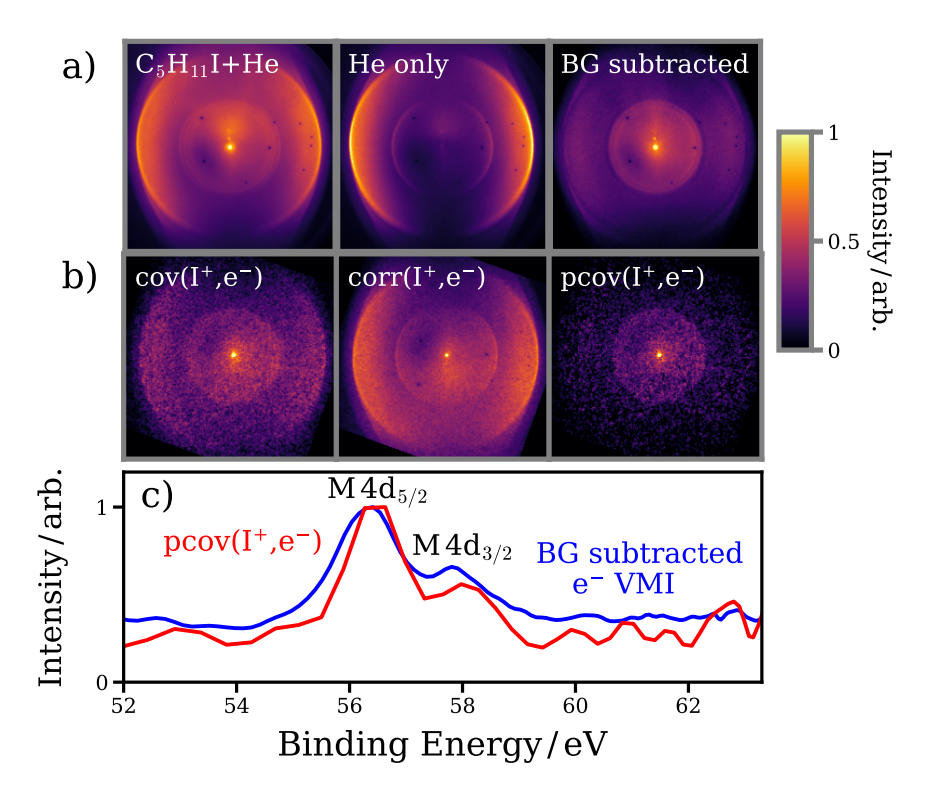


Figure 3: a) Photoelectron VMI images (UV-XUV) of: (left to right) 1-iodo-2-methylbutane seeded in He carrier gas, He only and 1-iodo-2-methylbutane following background subtraction. b) Electron-ion partial covariance analysis for the I⁺ ion, showing images of (left to right) covariance, correction term and the partial covariance. c) Electron spectra associated with the background subtracted velocity-map electron image (blue) and the I⁺ electron-ion partial covariance image (red). The two main features, arising from molecular $4d_{5/2}$ and $4d_{3/2}$ ionization, are labelled.

orbital compositions of the molecule in its ground state, but also potentially for the evolving composition of the chemical environment of the respective emitter site. For the static case of electron emitted from the I 4d site of $C_5H_{11}I$, the β_2 parameter 36,47 for electrons originating from the molecular I 4d site was determined to be $\beta_2 = 0.25$ for the $4d_{5/2}$ and $\beta_2 = 0.3$ for the $4d_{3/2}$, which is in reasonable agreement to previous work on CH_3I^{48} under the given experimental conditions and provides a benchmark for further studies. Following the time dependence of these angular distributions with partial covariance mapping during molecular dissociation is a goal for future (higher statistics) studies.

The electron velocity distributions correlated with production of a particular photoion 153 can be extracted by calculating the covariance between the integrated count of the ion of 154 interest and each pixel of the electron image. As three-dimensional ion-velocity information 155 is recorded on an shot-by-shot basis, electron spectra correlated to a specific range of ion 156 velocities can be calculated by appropriately selecting ions within a given velocity range. 157 Figure 3b) shows the electron-ion covariance calculated for the I⁺ ion, which is predomi-158 nantly produced following interaction of the molecule with the XUV pulse alone (see Figure 159 2a). In this image, which represents the laboratory-frame photoelectron distribution corre-160 lated to the production of I⁺ ions, the I 4d feature is clearly highlighted. However, there is still significant background present from the He seeding gas. This 'false' covariance is at-162 tributed to correlations induced by the fluctuating FEL power during the experiment, which 163 has the effect of correlating all measured signals. This can be accounted for through partial 164 covariance analysis 24,25,49 as the FEL pulse energy is also recorded on a shot-by-shot basis 50 165 (details of the partial covariance procedure are given in the Methods section). An additional 166 map, denoted the 'correction' map, representing the (linear) correlations induced by the 167 fluctuating FEL pulse energy is constructed. Subtraction of this term from the covariance 168 term yields the partial covariance, which isolates the true electron-ion correlations (which, 169 in this case arise from ionizing at the I 4d orbital of 1-iodo-2-methylbutane). In panel c), 170 strong principal agreement is observed between the covariant electron spectrum for I⁺ and 171

the equivalent spectrum obtained following subtraction of the various background contributions from the raw electron image. We note that the photoelectron spectrum extracted 173 from the partial covariance image is noisier than the equivalent image obtained through 174 background subtraction of the raw electron image. This is in part due to the nature of the 175 covariance mapping procedure, which relies on statistical (Poisson) fluctuations in a noisy 176 dataset and the detection of multiple particles, each of which have rather finite detection 177 efficiencies. The influence of these factors on covariance mapping has been examined in 178 detail recently. 51,52 The covariant electron spectrum importantly contains information that 179 cannot be gleaned from the raw photoelectron spectra, namely channel-resolved information 180 by extracting photoelectron spectra correlated to the production of a given ion channel. 181

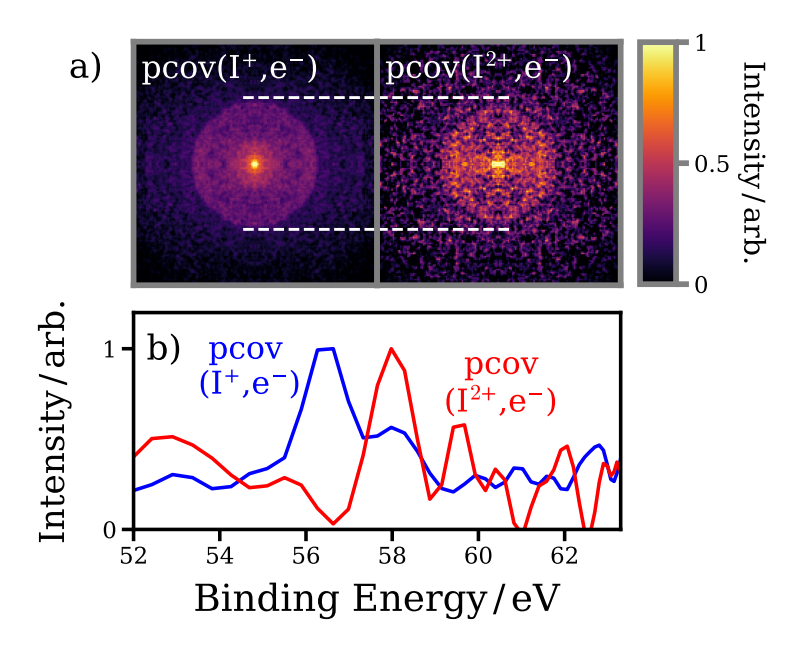


Figure 4: a) Electron-ion partial covariance images (symmetrized) for the I^+ ion and the I^{2+} ion (low radius ions only, for pump-probe delays of $+0.55\,\mathrm{ps}$ and $+0.80\,\mathrm{ps}$). A horizontal line at the radius of the ring seen in the I^+ image highlights the shift to lower radius in the I^{2+} case. b) Photoelectron spectra extracted from each of these partial covariance images.

As discussed previously, the low kinetic energy I²⁺ ions observed in Figure 2 are formed by a distinct pathway: UV-induced photodissociation and subsequent XUV ionization at the nascent iodine atom 4d orbital. The partial covariance image for low-velocity (i.e. originating

from neutral dissociation) I²⁺ ions is plotted in Figure 4(a), for long positive pump-probe delays (UV first by at least 550 fs). In Figure 2(a), a clear circular feature is observed at 186 a significantly lower radius (higher electron binding energy) than for XUV-only ionization 187 and fragmentation of the parent molecule. As seen in Figure 4b), the spectrum associated 188 with the neutral dissociation exhibits a shift to higher binding energies, by approximately 189 1.5 - 2 eV, consistent with synchrotron studies on the I 4d photoelectron spectra of free 190 iodine atoms. 44,45 Crucially, and in contrast to previous work, 7 this energetic shift as a 191 result of dissociation can be completely isolated from the far stronger unpumped parent 192 molecule signal, as well as from any competing pump-probe channels, such as the multiphoton 193 dissociative ionization pathway. As such, the method presented here allows for decisive 194 insights into the photochemistry of this prototypical molecule. 195

Figure 5 shows the covariant electron spectra associated with low-velocity I^{2+} ions in a 196 time-resolved manner. For all pump-probe delays, the electron spectra in covariance with 197 the I²⁺ photodissociation products show clear differences from the spectrum of ground state 198 molecules. Three main peaks can be seen in these spectra in the ~ 56 - $61\,\mathrm{eV}$ region, along 199 with an immediate, unresolved, shift to higher electron binding energies. In the ${\sim}54$ -200 56 eV region, the signal (with either negative or positive intensity) is assigned to the partial covariance routine failing to correctly remove all the He-background contributions. This 202 issue arises due to the relatively low statistics when calculating the partial covariance for a 203 given delay bin. The peak at ~ 56.5 eV visible in panel a) coincides energetically with the 204 signal stemming from the unpumped molecule, indicated by the I⁺ signal and displayed in 205 more detail in Figure 3 c). At small time delays, the overall yield of the I²⁺ is reduced since 206 charge transfer between the fragments can still happen. Therefore, the relevance of such a 207 contribution could be slightly enhanced, even in the covariance analysis. 208

In order to better understand the origins of these experimental observations, we have calculated photoelectron spectra as a function of carbon-iodine distance while keeping the remaining geometry parameters fixed, for the ${}^{3}Q_{0}$ and ${}^{1}Q_{1}$ excited states (a full description

209

210

211

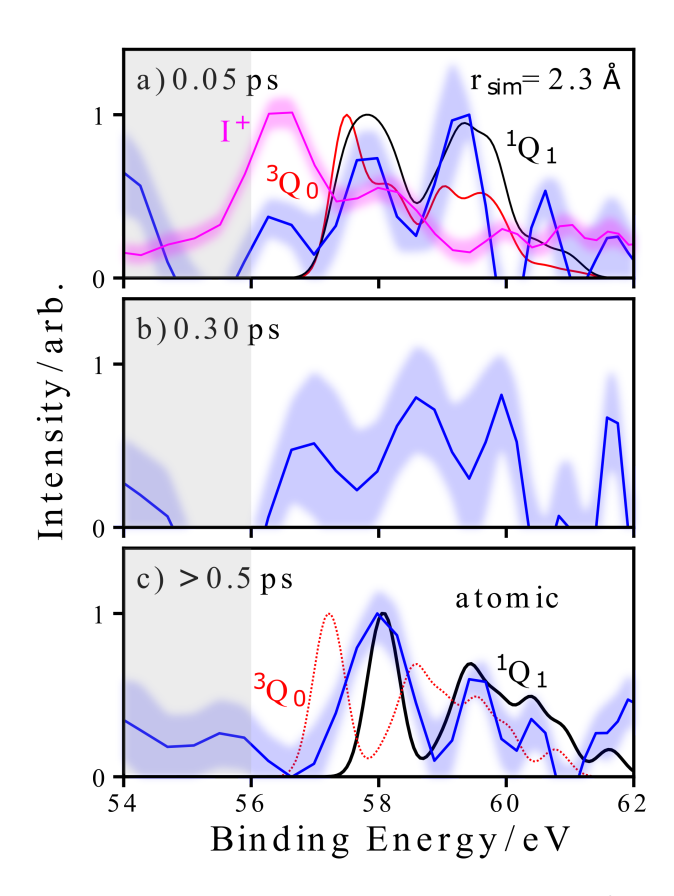


Figure 5: Angle-integrated electron spectra extracted from the I^{2+} electron-ion partial covariance images at a series of pump-probe delays in comparison to selected theoretical results. For each spectrum, the shaded area in blue represents errors at the 1σ level estimated from a bootstrapping analysis. The gray shaded area indicates a level of reduced confidence (see text). In panels a) and c), simulated spectra on the 3Q_0 (red) and 1Q_1 (black) potentials are shown in comparison to the experimental spectra (blue). In panel a), this is for a for C-I bond distance of 2.30 Å, whereas in c), the theoretical spectra are in the dissociated (i.e. atomic) limits. In panel a), the electron spectra extracted from the I^+ electron-ion partial covariance image is also shown (in magenta), representing the photoelectron spectrum of unpumped molecules.

of the theoretical methods is given in the Methods section). As in $\mathrm{CH_3I^{29,53}}$ and other iodoalkanes, ^{29,54–56} photoexcitation occurs predominantly to the ³Q₀ state, which correlates 213 to spin-orbit excited I* $(^{2}P_{1/2})$ products. ⁵⁷ This state is crossed by the $^{1}Q_{1}$ state, in our case 214 at around 2.4 Å C-I bond distance, correlating to ground state I (${}^{2}P_{3/2}$). From our classical 215 simulations of the C-I bond elongation (described in detail in the Methods section), which 216 reaches an asymptotic velocity of $\sim 25 \,\mathrm{\AA}\,\mathrm{ps}^{-1}$, this channel-crossing occurs at around 10 fs. 217 During the dissociation, significant population transfer from ${}^3\mathrm{Q}_0$ to ${}^1\mathrm{Q}_1$ occurs enabling 218 production of ground state I atoms. This is the dominant dissociation pathway, particularly 219 in larger alkyl iodides.^{29,58} In Figure 5, the time-resolved experimental data are compared 220 with theoretical spectra calculated close to the equilibrium bond distance (panel a)), and in 221 the long bond distance limit (panel c)) for both electronic states. Our theoretical work does 222 not consider any possible contributions from other excited states, which, in the case of the 223 related CH₃I molecule, are believed to have extremely low oscillator strengths at the pump 224 energy used.⁵⁹ 225

Although the time resolution of ± 100 fs precludes direct observation of the non-adiabatic 226 behavior at the conical intersection, ^{58,60,61} the comparison with theory is still illuminating. 227 At the earliest pump-probe delay, potential contributions from the initially populated ${}^{3}Q_{0}$ state and the ¹Q₁ state cannot be clearly distinguished, with qualitative indications for either state, consistent with some convolution of both involved states. For the second delay 230 at 300 fs, the evolution of the spectral dynamics (primarily on the ${}^{1}\mathrm{Q}_{1}$ state) is theoretically 231 predicted to be finished, which cannot be decisively confirmed by the present data. Whether 232 this observation is due to relatively poor statistics for this pump-probe delay, or indicates 233 some longer timescale dynamics (as have been recently observed in CH₃I following A-band 234 $excitation^{53,62}$) cannot be clearly concluded in the current data but will be investigated 235 further in future work. For long delays, in contrast, the dominant contribution can be 236 clearly assigned to the $^1\mathrm{Q}_1$ channel $(\mathrm{I}(^2\mathrm{P}_{3/2})),$ with any minor contributions from the $^3\mathrm{Q}_0$ 237 state causing a significantly smaller binding energy shift than that observed. 238

The current work demonstrates the applicability of electron-ion partial covariance imag-239 ing to ultrafast site-specific photoelectron spectroscopy. Future upgrades to FELs in terms 240 of repetition rate, polarization⁶³ and pulse duration⁶⁴ control, in combination with ultra-241 short optical laser pulses in particular in the UV regime, 65-67 and advanced camera readout 242 schemes, will enhance the data acquisition rate by orders of magnitude and can hence en-243 able robust determination of covariant electron angular distributions and their temporal 244 evolution. Experiments building on this methodology presented here will enable the study 245 of coupled nuclear electron dynamics, such as those associated with conical intersections, 246 in exquisite detail. Besides gaining first photochemical insights into the chiral molecule 247 1-iodo-2-methylbutane, our approach can also be readily extended to asymmetric angular 248 distributions, in either the laboratory- or recoil-frame which can provide a promising tool 249 for exploring ultrafast *chiral* dynamics. 250

$_{^{251}}$ Methods

252 Experiment

Experiments were performed at the beamline BL1 of FLASH 1,28 using the CAMP end-253 station. 27 The experimental setup consists of a dual-sided velocity-map-imaging spectrometer. Samples of R/S-1-iodo-2-methylbutane were introduced as a continuous molecular 255 beam, seeded in helium, which is collimated by two skimmers en route to the spectrometer's 256 interaction region. Here, molecules were crossed perpendicularly by focused UV and XUV 257 pulses provided by the FLASH pump-probe laser and FEL respectively. Linearly polarized 258 UV pulses (267 nm (4.6 eV), ~150 fs) were generated through third-harmonic generation of 259 the fundamental output of a Ti:Sapphire amplifier (Coherent Inc., Hydra), in a β-BaB₂O₄ 260 crystal. The resultant UV pulses were focused in the interaction chamber to a diameter of 261 about 100 μm , with attenuated pulse energies on the order of few μJ (maximum of 7 μJ), 262 and used to photoexcite the target molecules, ultimately initiating C-I bond cleavage. 263

XUV pulses (19.1 nm (63.5 eV), \sim 50 fs) generated by FLASH were used to probe the 264 ensuing molecular dynamics through photoionization, predominantly from the I 4d core 265 site. 30 The repetition rate was 10 Hz. The optical laser was blocked by a mechanical chopper 266 for 1 in every 10 pulses (i.e., at 1 Hz), to record background (XUV-only) data. These FEL 267 pulses were circularly polarized using the recently installed four-mirror reflection polarizer 268 in order to potentially enable stereochemical sensitivity. ⁶⁸ The resultant polarization of the 260 beam is determined by the angle of the mirror assembly, which can be adjusted via a stepper 270 motor. The estimated degree of circular polarization was $\sim 80\%$. The estimated averaged 271 energy bandwidth of the FEL pulses is approximately 1% FWHM ($\sim 0.60 \,\mathrm{eV}$), which is the 272 primary contribution to the energy uncertainty in the recorded photoelectron spectra. 273

The beamline transmission of BL1 at the chosen photon energy is $\sim 18\%,^{27}$ while the inserted polarizing mirrors have a reflectively of $\sim 68\%$. Typical FEL pulse energies were approximately $50 \,\mu\text{J}$, but were attenuated by a factor of ~ 5 using a 420 nm Al filter, in order to reduce contributions from multiphoton effects. Nickel-coated mirrors mounted in Kirkpatrick-Baez geometry focused the beam to about a diameter of about $10 \,\mu m$.

Following the interaction of target molecules with the focused laser and FEL pulses, the 279 generated ions and electrons are accelerated to position-sensitive MCP/phosphor screen detectors at the top and bottom of the instrument, respectively. Potentials were applied to the 281 ion optics such that velocity mapping conditions were met for both ions and electrons. ³¹ On 282 the ion side, the resultant light flashes at the phosphor are imaged by a fast-time-stamping 283 PImMS2 camera. 32,33 This employs a 324×324 pixel sensor capable of recording the spatial 284 coordinates (x, y) and arrival time (t) of events at high count rates. In the current experi-285 ment, the sensor was operated at a timing precision of 25 ns, which facilitates imaging of a 286 wide range of ions within a single experimental cycle. Velocity-map images corresponding to 287 a particular m/z value were extracted from the PImMS dataset by integrating over a char-288 acteristic time-of-flight range for the ion of interest. Multi-mass imaging allows momentum 289 correlations between ionic fragments to be determined using covariance analysis. ^{20,21,40} The 290

electron detector was gated in time by fast HV switches (Behlke) to minimize background contributions from stray light, and the electron images were captured using a 2448×2048 pixel CCD camera.

Ion and electron velocity-map images were recorded for several pump-probe delays be-294 tween the optical and free-electron lasers, as were relevant single-color and background 295 datasets. The fluctuations of the FEL timing and pulse energy on a shot-to-shot basis were 296 recorded using the FLASH Bunch Arrival Monitor ⁵⁰ and Gas Monitor Detector, ⁶⁹ respec-297 tively. Throughout the beamtime, data at several fixed pump-probe delays were recorded 298 by switching delays between individual (\sim 1-2 hour) data acquisition runs, to minimize the 290 effect of gradual drifts in experimental conditions on the data at a given pump-probe delay. 300 Frequently, acquisitions were also recorded whilst scanning the pump-probe delay in small 301 steps, in order to conclusively establish time-zero and thus verify stable timing between the 302 optical and FEL pulses. In order to improve the three-dimensional (x, y, t) resolution of 303 the ion-imaging data recorded by the PImMS camera, centroiding in time and space was performed. 40 305

306 Theoretical Methods

Theoretically, the cross section for ionizing from spin-orbit (SO) coupled states I to SO coupled state F were calculated as

$$\sigma_{\rm IF}(\omega) = \frac{4}{3} \alpha \pi^2 \omega \sum_{I'} \sum_{F'} |C_{I',I}|^2 |C_{F',F}|^2 \sum_{M=-1.0.1} \left| \langle \psi_{F'}^N | \hat{d}_M | \psi_{I'}^N \rangle \right|^2 \delta(E_F - E_I - \omega) \tag{1}$$

where α is the fine structure constant, $C_{I',I}$ and $C_{F',F}$ are the expansion coefficients of the initial and final SO coupled states in the non-SO coupled basis states $|\psi_{I'}^N\rangle$ and $|\psi_{F'}^N\rangle$, respectively, and $\delta(E_F - E_I - \omega)$ is a Gaussian broadening function with a standard deviation $_{312}$ of $0.212\,\mathrm{eV}$. The many electron dipole operator in Eq. 1 is

$$\langle \psi_{F'}^N | \hat{d}_M | \psi_{I'}^N \rangle = \sum_{i,j} \langle \psi_{F'}^N | c_i^{\dagger} c_j | \psi_{I'}^N \rangle \langle i | \hat{d}_M | j \rangle, \tag{2}$$

where c_i and c_j^{\dagger} are fermionic creation and annihilation operators and $\langle i|\hat{d}_M|j\rangle$ the dipole moment in the one-particle basis.

To calculate the transition dipole matrix elements for the basis states, $\left|\langle \psi_{F'}^N | \hat{d}_M | \psi_{I'}^N \rangle\right|^2$, we employed the one-center approximation, in which we separated the final electronic state $|\psi_{F'}^N\rangle$ into a bound part $|\psi_{F'}^{(N-1)}\rangle$ and a one electron continuum part ϕ_k . The respective continuum wave function ϕ_k was approximated with atomic continuum wave functions at the appropriate kinetic energy $k^2/2 = \omega - (E_F - E_I)$. More details on this procedure can be found in Ref. ^{70,71}

We obtained the expansion coefficients $C_{I',I}$ and $C_{F',F}$, as well as E_I and E_F from SO 321 calculations diagonalizing the Breit-Pauli Hamiltonian in the space of the initial and final 322 basis states $\psi_{I'}^N$ and $\psi_{F'}^{(N-1)}$, respectively. In particular, we conducted a state-averaged com-323 plete active space (SA-CASSCF) calculation involving an orbital space of 4 orbitals with 324 6 electrons for an equal-weighted average over the 3 lowest singlet states employing the 6-325 311G(d,p) basis set. 72,73 With the obtained set of orbitals, we constructed a set of basis 326 states for the SO calculations for the initial, neutral state consisting of the 6 lowest triplet 327 and 4 lowest singlet states obtained by diagonalizing the CI matrix in this active space. For 328 the final state, we took into account the full spectrum of states constructed by diagonalizing 329 the CI Matrix in the employed active space with an additional hole in the 4d shell resulting in 80 doublet and 30 quadruplet states. The SO coefficients $C_{I,I'}$ and $C_{F,F'}$ as well as the 331 respective energetic position of the SO-coupled states were calculated using molpro version 332 2020.1.⁷⁴ The cross sections were calculated using the XMOLECULE toolkit.^{70,75} 333

To calculate the molecular photoelectron spectrum, we employed a common orbital set for the initial, neutral, and final 4d-ionized states. Because orbital relaxation effects due to

the presence of the 4d hole are not taken into account, the energy differences between initial and final states are somewhat too large. This effect has been estimated from a calculation for 337 atomic iodine where the orbital relaxation effect was considered. We find that the inclusion of 338 relaxation effects results in a spectral shift of $\sim 5\,\mathrm{eV}$ and only minor changes in the spectral 339 shape. We further note that discrepancies to the experimental spectra may also arise due 340 to missing relativistic effects and the limited size of the employed basis set. To correct for 341 these effects and facilitate a comparison with the experimental data, we additionally shifted 342 the calculated photoelectron binding energies by 1.4 eV towards lower energies. 343

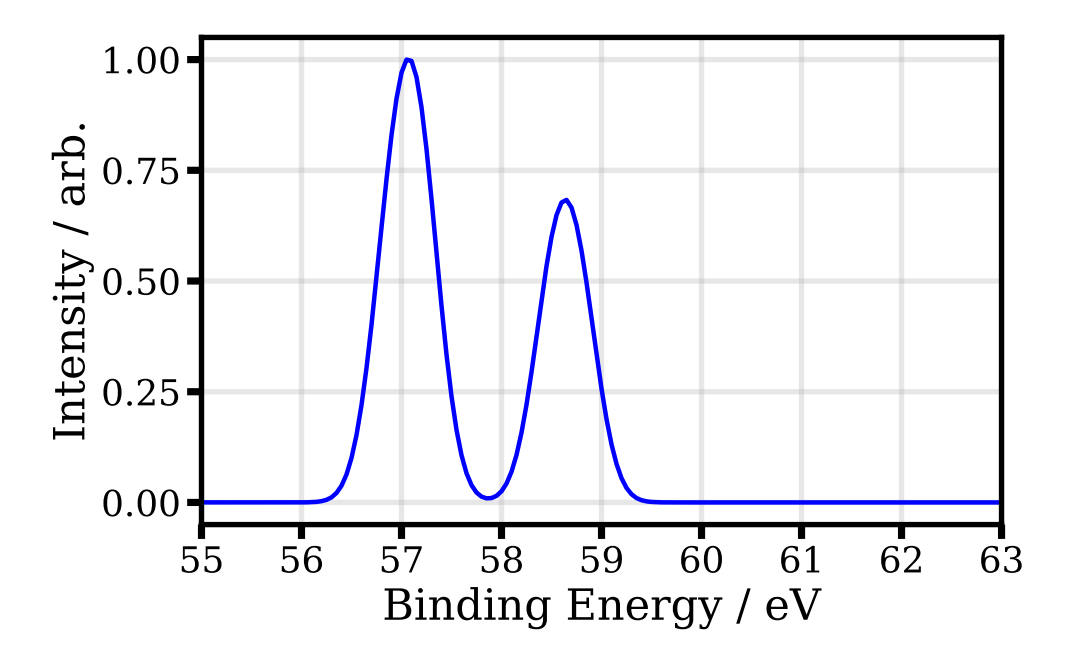


Figure 6: Calculated photoelectron spectrum of the 4d level of the molecule (ground state).

Figure 6 shows the calculated spectrum for the molecular electronic ground state. As 344 can be seen, the calculation shows the expected SO splitting of $\sim 1.7\,\mathrm{eV}$ between the two 345 levels $4d_{5/2}$ and $4d_{3/2}$ levels.⁷⁶ 346

For the excited state, we have calculated the photoelectron spectrum as a function of 347 iodine carbon distance, keeping the remaining geometry parameters fixed. Specifically, we 348 show spectra, for the excited ${}^{3}Q_{0}$ and ${}^{1}Q_{1}$ state, that are relevant for the photoinduced dissociation dynamics. Figure 7 shows the calculated potential energy curves. The 3Q_0 state 350

349

correlates asymptotically to the excited iodine fragment in ${}^2P_{1/2}$ configuration (I*), the 1Q_1 state corresponds to the iodine in its ${}^2P_{3/2}$ ground state. As can be seen, both potential energy curves cross at $\sim 2.4 \,\text{Å}$.

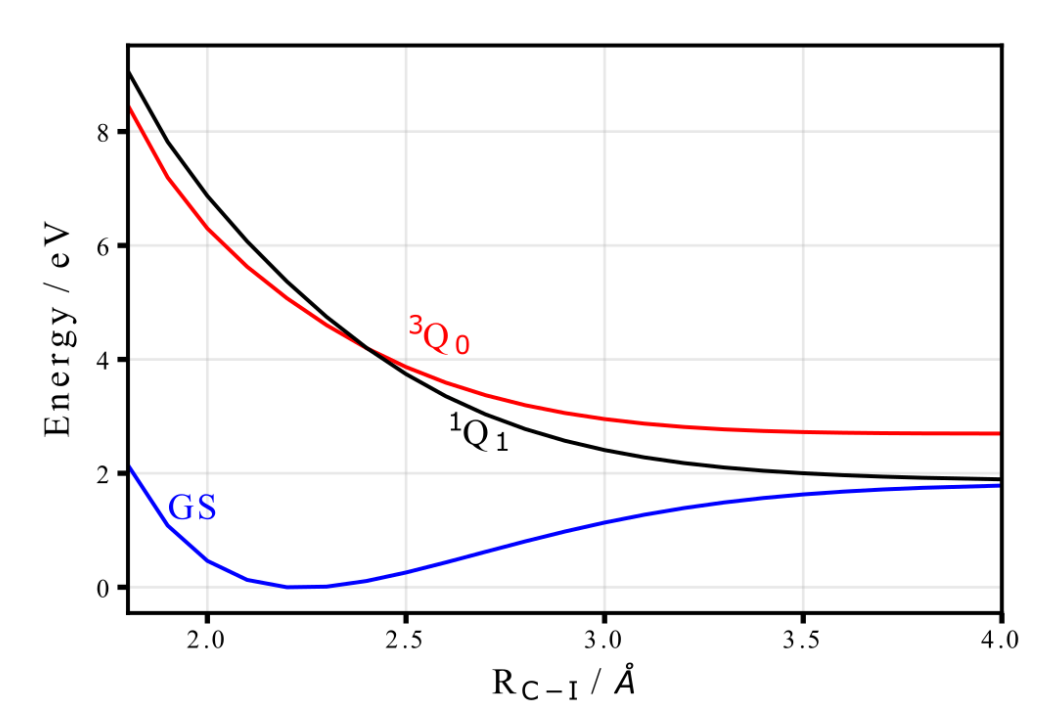


Figure 7: Calculated potential energy curves for the ground and selected excited states of the molecule along the C-I bond.

The calculated 4d photoelectron spectrum as a function of internuclear distance is shown in Figure 8 for the 3Q_0 state and in Figure 9 for the 1Q_1 state. With increasing interatomic distance, one can see that both spectra initially move to lower binding energies and exhibit only slight changes beyond an internuclear C-I distance of 3.5 Å. The 3Q_0 photoelectron spectrum at large internuclear distances is roughly 0.9 eV lower compared to the 1Q_1 photoelectron spectrum. As expected from the asymptotic dissociation limit, the 3Q_0 spectrum corresponds to the atomic I* photoelectron spectrum at large internuclear distances, whereas the 1Q_1 spectrum corresponds to the atomic I ground state photoelectron spectrum.

To qualitatively assess the dynamics triggered by the initial excitation, we conducted an MD simulation. Starting from the Franck-Condon geometry of the molecule, the trajectories were propagated on the lowest triplet excited state using the TD-DFT method employing

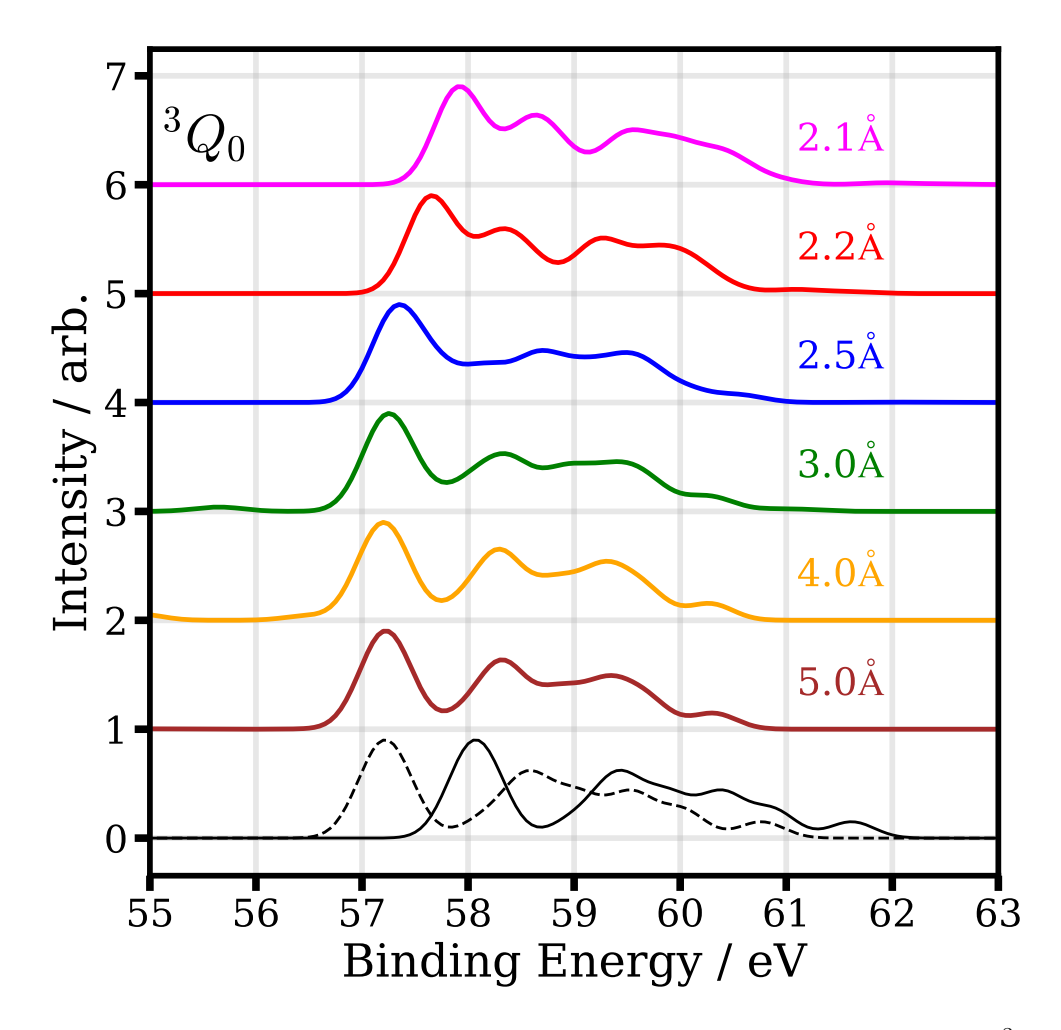


Figure 8: Calculated photoelectron spectrum of the 4d level of the molecule (${}^{3}Q_{0}$ excited state) for selected interatomic distances. The two lowest lines show the calculated spectra for atomic iodine in its ground (black, solid line) and excited state (black, dotted line).

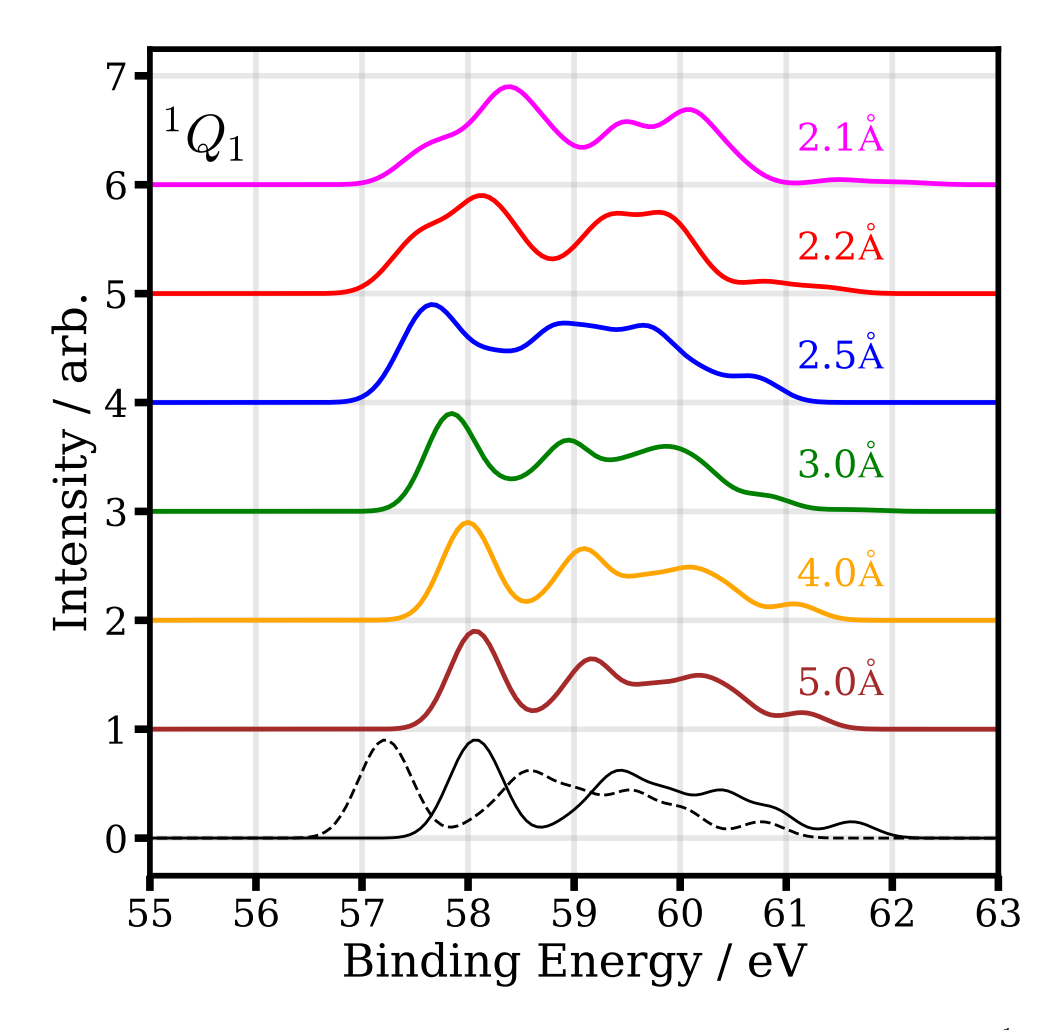


Figure 9: Calculated photoelectron spectrum of the 4d level of the molecule (${}^{1}Q_{1}$ excited state) for selected interatomic distances. The two lowest lines show the calculated spectra for atomic iodine in its ground state (black, solid line) and excited state (black, dotted line).

the SBKJC effective-core potential basis set ⁷⁷ using GAMESS. ⁷⁸ As we described in the main text, we observe that the C-I bond distance almost linearly increases with a speed of $\simeq 25 \text{Å ps}^{-1}$ in accordance with earlier results for similar iodoalkanes. ²⁹ We see that the conical intersection at 2.4 Å is reached within $\simeq 10 \text{ fs}$, as displayed in Figure 10.

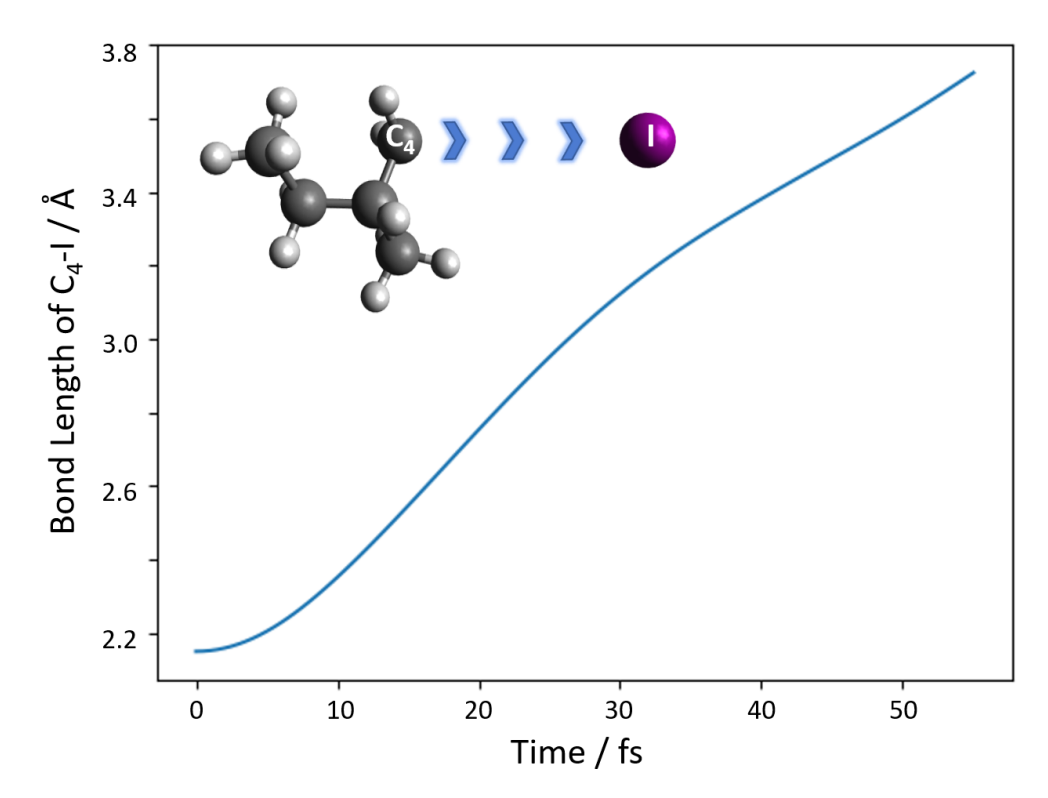


Figure 10: Simulation of the bond-length elongation between the closest carbon (C_4) and the iodine atom.

${f Assignment~of~Time~Zero}$

In experiments incorporating a weak-field UV pump and an XUV probe, it is often difficult to precisely assign time-zero. 4,7,8,79 For instance, analysis of the low KE, neutral photodissociation feature observed in the I²⁺ ion signal in the current work is complicated by the fact that the feature's time-evolution depends on delay-dependent (and therefore distance-dependent) charge-transfer probabilities following photoexcitation. As a result, in the present experiment, time-zero is determined from the delay-dependent intensity of the higher KE feature observed in the I²⁺ ion signal, whose KE decreases at longer pump-probe delays. As men-

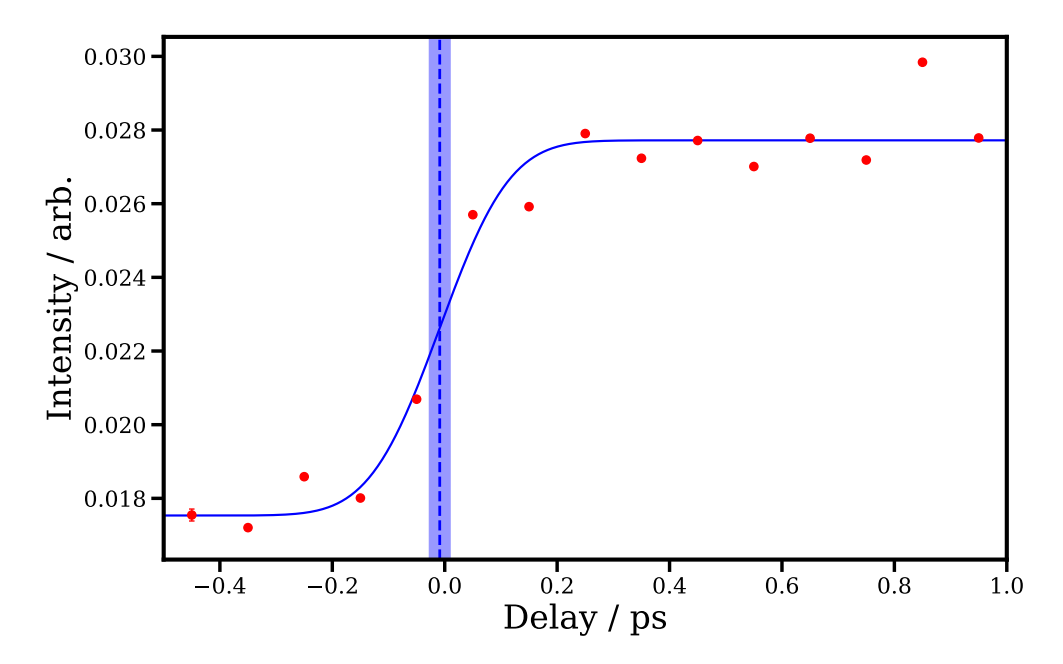


Figure 11: Pump-probe delay-dependent intensity (red points) of the I^{2+} 'Coulomb curve' feature. A Gaussian cumulative distribution function (CDF) fit to this is shown in blue. The centre of this fit is marked by a blue dashed line, and the standard fitting error of this parameter is marked by the shaded blue region.

tioned in the main text, this feature arises from a multiphoton UV dissociative ionization to yield a cationic alkyl fragment, before XUV ionization at the neutral iodine fragment. As we expect this channel to be observed immediately following UV excitation, and charge-transfer is much less favorable to an already charged alkyl fragment (and thus less likely to affect the yield of this channel), we take the center of the rise of this channel as the point at which the two pulses are temporally overlapped. The intensity of this feature as a function of pump-probe delay, and a fit to this, from which the time-zero may be extracted, is shown in Figure 11.

385 Error Estimation

Figure 4 of the main manuscript displays the delay-dependent electron spectra in partial covariance with the I^{2+} ion. Estimated errors of these spectra (1σ) are also given, represented as shaded areas. These errors were determined using a bootstrapping analysis of the data.

The data used to generate each spectrum was originally recorded as multiple distinct data

acquisitions (each of tens of thousands of laser shots) during the original FEL beamtime.
For each pump-probe delay, these individual data acquisitions were randomly sampled (with replacement), to generate a new dataset, from which the electron-ion partial covariances were calculated. This process was repeated many times, and the standard deviation from the many spectra was used as an estimate of the overall statistical error.

Electron-Ion Partial Covariance Calculation

Covariance, a measure of linear correlation between two variables, X and Y, is defined as: 20

$$Cov(X,Y) = \langle XY \rangle - \langle X \rangle \langle Y \rangle \tag{3}$$

where arithmetic means are taken over a series of observations (in our case, laser shots). In the present work, prior to calculation of the covariance, some data filtering was performed. Firstly, only laser shots in which both the UV and XUV lasers irradiated the sample were selected. Secondly, FEL pulses with outlying pulse energies (more than 1.5σ away from the mean pulse energy) were removed. The covariance was then calculated between each pixel of the electron image (recorded on a shot-to-shot basis) and the total count of the ion channel in interest, derived from the centroided PImMS camera data. Such a covariance image is shown in the left-hand side of Figure 2b) of the main manuscript.

The calculated covariance images still feature signal which is not correlated to the ion of interest. This 'false covariance' arises due to the fluctuating FEL power during the experiment, as described in the main text. To account for this, partial covariance is calculated, ²⁵ in which an additional correction term, representing these (linear) correlations induced by the fluctuating power, is calculated. This term is defined as:

$$Corr(X, Y; I) = \frac{Cov(Y, I)Cov(I, X)}{Cov(I, I)}$$
(4)

The correction term is calculated using the FEL pulse energy measured by the FLASH Gas

Monitor Detector⁵⁰ as the fluctuating parameter. The correction term is calculated by determining the covariance between the FEL pulse energy and the ion count, as well as the 412 covariance between the FEL pulse energy and each pixel of the electron image, as seen in 413 Equation 4. Once the correction term is subtracted from the covariance, the partial covari-414 ance remains. Example correction and partial covariance images are shown in the centre and 415 right-hand portions of Figure 2b) in the main manuscript. The covariant electron spectra 416 presented in the main manuscript are obtained by Abel-inverting the electron-ion partial 417 covariance images (using the pBASEX³⁵ algorithm). The presented spectra are normalized 418 to unit peak intensity in the spectral region of interest. 419

420

421

Data availability

The data that support the findings of this study are available from the corresponding author on reasonable request. All steps to reproduce the presented experimental and theoretical findings are either explained in detail or cited in the manuscript.

425

426

Competing interest

The authors declare no competing interest.

428

429

Acknowledgments

We gratefully acknowledge DESY for provision of the free-electron laser beamtime at the BL1
CAMP endstation of FLASH as well as the work and sedulous support of the scientific and
technical teams. FA, MB, DH, RM and CV acknowledge funding from EPSRC Programme
Grants EP/L005913/1 and EP/T021675/1. MBu is grateful for support from the UK EPSRC (EP/S028617/1 and EP/L005913/1). This work was partly funded by the Deutsche
Forschungsgemeinschaft (DFG)-Project No. 328961117-SFB 1319 ELCH (Extreme light
for sensing and driving molecular chirality). We furthermore acknowledge the Max Planck
Society for funding the development and the initial operation of the CAMP end-station

within the Max Planck Advanced Study Group at CFEL and for providing this equipment for CAMP@FLASH. The installation of CAMP@FLASH was partially funded by the BMBF grants 05K10KT2, 05K13KT2, 05K16KT3 and 05K10KTB from FSP-302. MI, VM, and PhS acknowledge funding by the Volkswagen Foundation within a Peter-Paul-Ewald Fellowship. SD, KS, LS, and SB acknowledge funding from the Helmholtz Initiative and Networking Fund through the Young Investigators Group Program (VH-NG-1104). Furthermore, KS and SB were supported by the Deutsche Forschungsgemeinschaft, project B03 in the SFB 755 - Nanoscale Photonic Imaging. DRo was supported by the US National Science Foundation through grant PHYS-1753324.

448 Author contributions

447

MI conceived and proposed the experiment. The experiment was performed by FA, VM, 440 RB, BE, PhS, TMB, MBu, SD, PG, DH, ML, JWLL, LM, RM, HO, CP, DRo, KS, LS, RW, 450 VZ, SB, and MI. The optical laser system was operated and adjusted by BM, RB, BE, and 451 PG with support in the design by AG. Engineering support including modifications to the 452 spectrometer was provided by BE, and DR. The R-enantiomer of the target was synthesized 453 and provided by RP, DK, and IV. FA analyzed the data with further contributions during the beamtime from PhS, LM, CP, and SD. The electron-ion partial covariance methods were developed by FA with insight from MB and MI. LI and ZL performed the theoretical 456 calculations. CvKS has set-up and supported the operation of the polarizing mirrors. FA, 457 VM, LI, RB, BE, PhS, TMB, GB, MBu, PhD, SD, AE, AG, PG, DH, DK, ML, JWLL, ZL, 458 BM, LM, RM, MM, HO, CP, RP, DR, DRo, KS, LS, RT, CV, IV, CvKS, RW, PW, VZ, SB, 459 MB, and MI contributed to in-depth discussions and interpretation. FA, LI, and MI wrote 460 the manuscript with dedicated contributions by ZL. 461

References

- (1) Zewail, A. H. Femtochemistry: Atomic-Scale Dynamics of the Chemical Bond. J. Phys.

 Chem. A 2000, 104, 5660-5694.
- 465 (2) Erk, B. et al. Inner-shell multiple ionization of polyatomic molecules with an intense 466 x-ray free-electron laser studied by coincident ion momentum imaging. J. Phys. B At. 467 Mol. Opt. Phys. 2013, 46, 164031.
- 468 (3) Erk, B. et al. Imaging charge transfer in iodomethane upon x-ray photoabsorption.

 469 Science 2014, 345, 288–291.
- (4) Boll, R.; Erk, B.; Coffee, R.; Trippel, S.; Kierspel, T.; Bomme, C.; Bozek, J. D.; Burkett, M.; Carron, S.; Ferguson, K. R., et al. Charge transfer in dissociating iodomethane and fluoromethane molecules ionized by intense femtosecond X-ray pulses. *Structural Dynamics* **2016**, *3*, 043207.
- Wernet, P.; Leitner, T.; Josefsson, I.; Mazza, T.; Miedema, P. S.; Schröder, H.; Beye, M.;
 Kunnus, K.; Schreck, S.; Radcliffe, P.; Düsterer, S.; Meyer, M.; Odelius, M.; Föhlisch, A.
 Communication: Direct evidence for sequential dissociation of gas-phase Fe(CO)₅ via
 a singlet pathway upon excitation at 266 nm. J. Chem. Phys. 2017, 146, 211103.
- 478 (6) Leitner, T.; Josefsson, I.; Mazza, T.; Miedema, P. S.; Schröder, H.; Beye, M.; Kunnus, K.; Schreck, S.; Düsterer, S.; Föhlisch, A.; Meyer, M.; Odelius, M.; Wernet, P.

 Time-resolved electron spectroscopy for chemical analysis of photodissociation: Photoelectron spectra of Fe(CO)₅, Fe(CO)₄, and Fe(CO)₃. J. Chem. Phys. **2018**, 149, 044307.
- 483 (7) Brauße, F. et al. Time-resolved inner-shell photoelectron spectroscopy: From a bound
 484 molecule to an isolated atom. *Phys. Rev. A* **2018**, *97*, 043429.

- 485 (8) Forbes, R. et al. Time-resolved site-selective imaging of predissociation and charge 486 transfer dynamics: The CH3I B-band. *Journal of Physics B: Atomic, Molecular and* 487 *Optical Physics* **2020**, *53*, 13.
- 488 (9) Li, X.; Inhester, L.; Osipov, T.; Boll, R.; Coffee, R.; Cryan, J.; Gatton, A.;
 489 Gorkhover, T.; Hartman, G.; Ilchen, M., et al. Electron-ion coincidence measurements
 490 of molecular dynamics with intense X-ray pulses. *Scientific reports* **2021**, *11*, 1–12.
- (10) Mazza, T.; Ilchen, M.; Kiselev, M.; Gryzlova, E.; Baumann, T.; Boll, R.; De Fanis, A.;
 Grychtol, P.; Montaño, J.; Music, V., et al. Mapping Resonance Structures in Transient
 Core-Ionized Atoms. *Physical Review X* 2020, 10, 041056.
- (11) Davies, J. A.; LeClaire, J. E.; Continetti, R. E.; Hayden, C. C. Femtosecond time resolved photoelectron-photoion coincidence imaging studies of dissociation dynamics.
 J. Chem. Phys. 1999, 111, 1–4.
- (12) Boguslavskiy, A. E.; Mikosch, J.; Gijsbertsen, A.; Spanner, M.; Patchkovskii, S.;
 Gador, N.; Vrakking, M. J.; Stolow, A. The multielectron ionization dynamics underlying attosecond strong-field spectroscopies. *Science* 2012, 335, 1336–1340.
- 500 (13) Forbes, R.; Boguslavskiy, A. E.; Wilkinson, I.; Underwood, J. G.; Stolow, A. Excited 501 state wavepacket dynamics in NO₂ probed by strong-field ionization. *J. Chem. Phys.* 502 **2017**, *147*, 054305.
- 503 (14) Continetti, R. E. Coincidence spectroscopy. *Annu. Rev. Phys. Chem.* **2001**, *52*, 165– 504 192.
- (15) Arion, T.; Hergenhahn, U. Coincidence spectroscopy: Past, present and perspectives.
 Journal of Electron Spectroscopy and Related Phenomena 2015, 200, 222–231.
- $_{507}$ (16) Schnorr, K. et al. Electron Rearrangement Dynamics in Dissociating I_2^{n+} Molecules

- Accessed by Extreme Ultraviolet Pump-Probe Experiments. *Phys. Rev. Lett.* **2014**, 113, 073001.
- (17) Kastirke, G. et al. Double Core-Hole Generation in O₂ Molecules Using an X-Ray Free Electron Laser: Molecular-Frame Photoelectron Angular Distributions. *Phys. Rev. Lett.* 2020, 125, 163201.
- 513 (18) Kastirke, G. et al. Photoelectron Diffraction Imaging of a Molecular Breakup Using an

 514 X-Ray Free-Electron Laser. *Phys. Rev. X* **2020**, *10*, 021052.
- (19) Decking, W.; Abeghyan, S.; Abramian, P.; Abramsky, A.; Aguirre, A.; Albrecht, C.;
 Alou, P.; Altarelli, M.; Altmann, P.; Amyan, K., et al. A MHz-repetition-rate hard X-ray free-electron laser driven by a superconducting linear accelerator. *Nature Photonics* 2020, 1–7.
- 519 (20) Frasinski, L. J.; Codling, K.; Hatherly, P. A. Covariance Mapping: A Correlation
 520 Method Applied to Multiphoton Multiple Ionization. Science 1989, 246, 1029–1031.
- 521 (21) Frasinski, L. J. Covariance mapping techniques. J. Phys. B **2016**, 49, 152004.
- Peschel, J.; Wikmark, H.; Rudawski, P.; Gisselbrecht, M.; Johnsson, P. A Versatile Velocity Map Ion-Electron Covariance Imaging Spectrometer for High-Intensity XUV Experiments. *Appl. Sci.* **2018**, *8*, 998.
- Driver, T.; Cooper, B.; Ayers, R.; Pipkorn, R.; Patchkovskii, S.; Averbukh, V.;
 Klug, D. R.; Marangos, J. P.; Frasinski, L. J.; Edelson-Averbukh, M. Two-Dimensional
 Partial-Covariance Mass Spectrometry of Large Molecules Based on Fragment Correlations. *Physical Review X* 2020, 10, 041004.
- 530 (24) Kornilov, O. et al. Coulomb explosion of diatomic molecules in intense XUV fields
 531 mapped by partial covariance. J. Phys. B At. Mol. Opt. Phys. **2013**, 46, 164028.

- 532 (25) Frasinski, L. J. et al. Dynamics of hollow atom formation in intense X-ray pulses probed 533 by partial covariance mapping. *Phys. Rev. Lett.* **2013**, *111*, 073002.
- ⁵³⁴ (26) Zhaunerchyk, V.; Frasinski, L. J.; Eland, J. H.; Feifel, R. Theory and simulations of
 covariance mapping in multiple dimensions for data analysis in high-event-rate experi ments. Phys. Rev. A At. Mol. Opt. Phys. 2014, 89, 1–8.
- 537 (27) Erk, B. et al. CAMP@FLASH: an end-station for imaging, electron- and ion-538 spectroscopy, and pump-probe experiments at the FLASH free-electron laser. *J. Syn-*539 chrotron Radiat. **2018**, 25, 1529–1540.
- 540 (28) Ackermann, W. et al. Operation of a free-electron laser from the extreme ultraviolet to 541 the water window. *Nat. Photonics* **2007**, *1*, 336–342.
- Corrales, M. E.; Loriot, V.; Balerdi, G.; González-Vázquez, J.; De Nalda, R.;
 Bañares, L.; Zewail, A. H. Structural dynamics effects on the ultrafast chemical bond
 cleavage of a photodissociation reaction. *Phys. Chem. Chem. Phys.* 2014, 16, 8812–8818.
- oliney, T. N.; Cooper, G.; Brion, C. E. Quantitative studies of the photoabsorption (4.5-488 eV) and photoionization (9-59.5 eV) of methyl iodide using dipole electron impact techniques. *Chem. Phys.* **1998**, *232*, 211–237.
- (31) Eppink, A. T. J. B.; Parker, D. H. Velocity map imaging of ions and electrons using
 electrostatic lenses: Application in photoelectron and photofragment ion imaging of
 molecular oxygen. Rev. Sci. Instrum. 1997, 68, 3477–3484.
- Nomerotski, A.; Adigun-Boaye, S.; Brouard, M.; Campbell, E.; Clark, A.; Crooks, J.;
 John, J.; Johnsen, A.; Slater, C.; Turchetta, R.; Vallance, C.; Wilman, E.; Yuen, W.
 Pixel imaging mass spectrometry with fast silicon detectors. Nucl. Instruments Methods
 Phys. Res. Sect. A Accel. Spectrometers, Detect. Assoc. Equip. 2011, 633, S243-S246.

- John, J. J. et al. PImMS, a fast event-triggered monolithic pixel detector with storage of multiple timestamps. J. Instrum. **2012**, 7, C08001–C08001.
- (34) Inhester, L.; Li, Z.; Zhu, X.; Medvedev, N.; Wolf, T. J. Spectroscopic Signature of
 Chemical Bond Dissociation Revealed by Calculated Core-Electron Spectra. J. Phys.
 Chem. Lett. 2019, 10, 6536–6544.
- Garcia, G. A.; Nahon, L.; Powis, I. Two-dimensional charged particle image inversion
 using a polar basis function expansion. Rev. Sci. Instrum. 2004, 75, 4989–4996.
- 563 (36) Cooper, J.; Zare, R. N. Angular distribution of photoelectrons. *The Journal of chemical*564 physics **1968**, 48, 942–943.
- 565 (37) Zare, R. N. Angular Momentum; Wiley, 1988.
- Yang, S.-c.; Bersohn, R. Theory of the angular distribution of molecular photofragments. The Journal of Chemical Physics 1974, 61, 4400–4407.
- Allum, F.; Anders, N.; Brouard, M.; Bucksbaum, P.; Burt, M.; Downes-Ward, B.;
 Grundmann, S.; Harries, J.; Ishimura, Y.; Iwayama, H., et al. Multi-channel photodis sociation and XUV-induced charge transfer dynamics in strong-field-ionized methyl
 iodide studied with time-resolved recoil-frame covariance imaging. Faraday Discussions
 2021, 228, 571–596.
- 573 (40) Slater, C. S.; Blake, S.; Brouard, M.; Lauer, A.; Vallance, C.; John, J. J.; Turchetta, R.;

 574 Nomerotski, A.; Christensen, L.; Nielsen, J. H.; Johansson, M. P.; Stapelfeldt, H. Co
 575 variance imaging experiments using a pixel-imaging mass-spectrometry camera. *Phys.*576 *Rev. A* **2014**, *89*, 011401.
- (41) Slater, C. S.; Blake, S.; Brouard, M.; Lauer, A.; Vallance, C.; Bohun, C. S.; Christensen, L.; Nielsen, J. H.; Johansson, M. P.; Stapelfeldt, H. Coulomb-explosion imaging
 using a pixel-imaging mass-spectrometry camera. *Phys. Rev. A* 2015, *91*, 053424.

- ⁵⁸⁰ (42) Allum, F. et al. Coulomb explosion imaging of CH₃I and CH₂CII photodissociation ⁵⁸¹ dynamics. J. Chem. Phys. **2018**, 149, 204313.
- Grimm, F. A. Angle resolved photoelectron spectroscopy of the valence shells in HI and CH₃I as a function of photon energy from 13 to 90 eV. *J. Chem. Phys.* **1984**, 80, 3521–3527.
- Tremblay, J.; Larzilliere, M.; Combet-Farnoux, F.; Morin, P. Photoelectron spectroscopy of atomic iodine produced by laser photodissociation. *Phys. Rev. A* **1988**, 38, 3804–3807.
- 589 (45) Nahon, L.; Svensson, A.; Morin, P. Experimental study of the 4 d ionization continuum 590 in atomic iodine by photoelectron and photoion spectroscopy. *Phys. Rev. A* **1991**, 43, 591 2328–2337.
- ⁵⁹² (46) Holland, D.; Powis, I.; Öhrwall, G.; Karlsson, L.; von Niessen, W. A study of the photoionisation dynamics of chloromethane and iodomethane. *Chem. Phys.* **2006**, *326*, 535–550.
- (47) Schmidt, V. Photoionization of atoms using synchrotron radiation. Reports on Progress
 in Physics 1992, 55, 1483.
- 597 (48) Lindle, D.; Kobrin, P.; Truesdale, C.; Ferrett, T.; Heimann, P.; Kerkhoff, H.; Becker, U.;
 598 Shirley, D. Inner-shell photoemission from the iodine atom in CH₃I. *Physical Review A*599 **1984**, 30, 239.
- Mucke, M. et al. Covariance mapping of two-photon double core hole states in C_2H_2 and C_2H_6 produced by an x-ray free electron laser. New J. Phys. **2015**, 17, 073002.
- 602 (50) Tiedtke, K. et al. Gas detectors for x-ray lasers. J. Appl. Phys. **2008**, 103, 094511.

- (51) Mikosch, J.; Patchkovskii, S. Coincidence and covariance data acquisition in photo electron and -ion spectroscopy. I. Formal theory. Journal of Modern Optics 2013, 60,
 1426–1438.
- (52) Mikosch, J.; Patchkovskii, S. Coincidence and covariance data acquisition in photoelectron and -ion spectroscopy. II. Analysis and applications. *Journal of Modern Optics* 2013, 60, 1439–1451.
- (53) Downes-Ward, B.; Warne, E. M.; Woodhouse, J.; Parkes, M.; Springate, E.; Pearcy, P.;
 Zhang, Y.; Karras, G.; Wyatt, A.; Chapman, R., et al. Photodissociation dynamics of
 methyl iodide across the A-band probed by femtosecond extreme ultraviolet photoelectron spectroscopy. Journal of Physics B: Atomic, Molecular and Optical Physics 2021,
 54, 134003.
- 614 (54) Boschi, R.; Salahub, D. The far ultra-violet spectra of some 1-iodoalkanes. *Molecular*615 Physics **1972**, 24, 289–299.
- (55) Todt, M. A.; Datta, S.; Rose, A.; Leung, K.; Davis, H. F. Subpicosecond HI elimination
 in the 266 nm photodissociation of branched iodoalkanes. *Physical Chemistry Chemical Physics* 2020, 22, 27338–27347.
- (56) Ross, P. L.; Johnston, M. V. Excited state photochemistry of iodoalkanes. The Journal
 of Physical Chemistry 1995, 99, 4078–4085.
- (57) Mulliken, R. S. Intensities in Molecular Electronic Spectra X. Calculations on Mixed Halogen, Hydrogen Halide, Alkyl Halide, and Hydroxyl Spectra. The Journal of Chemical Physics 1940, 8, 382–395.
- 624 (58) Chang, K. F.; Reduzzi, M.; Wang, H.; Poullain, S. M.; Kobayashi, Y.; Barreau, L.;
 625 Prendergast, D.; Neumark, D. M.; Leone, S. R. Revealing electronic state-switching
 626 at conical intersections in alkyl iodides by ultrafast XUV transient absorption spec627 troscopy. Nat. Commun. 2020, 11, 4042.

- 628 (59) Eppink, A. T.; Parker, D. H. Methyl iodide A-band decomposition study by photofrag-629 ment velocity imaging. *Journal of Chemical Physics* **1998**, *109*, 4758–4767.
- (60) Chang, K. F.; Wang, H.; Poullain, S. M.; Prendergast, D.; Neumark, D. M.; Leone, S. R.
 Mapping wave packet bifurcation at a conical intersection in CH₃I by attosecond XUV
 transient absorption spectroscopy. The Journal of Chemical Physics 2021, 154, 234301.
- (61) Jadoun, D.; Kowalewski, M. Time-Resolved Photoelectron Spectroscopy of Conical
 Intersections with Attosecond Pulse Trains. The Journal of Physical Chemistry Letters
 2021, 12, 8103-8108.
- (62) Warne, E. M.; Downes-Ward, B.; Woodhouse, J.; Parkes, M. A.; Bellshaw, D.;
 Springate, E.; Majchrzak, P.; Zhang, Y.; Karras, G.; Wyatt, A. S., et al. Photodissociation dynamics of CH 3 I probed via multiphoton ionisation photoelectron spectroscopy.
 Physical Chemistry Chemical Physics 2019, 21, 11142–11149.
- Lutman, A. A.; MacArthur, J. P.; Ilchen, M.; Lindahl, A. O.; Buck, J.; Coffee, R. N.;
 Dakovski, G. L.; Dammann, L.; Ding, Y.; Dürr, H. A., et al. Polarization control in an
 X-ray free-electron laser. Nature photonics 2016, 10, 468–472.
- 643 (64) Duris, J. et al. Tunable isolated attosecond X-ray pulses with gigawatt peak power from
 a free-electron laser. Nat. Photonics **2020**, 14, 30–36.
- Reiter, F.; Graf, U.; Serebryannikov, E. E.; Schweinberger, W.; Fiess, M.; Schultze, M.;
 Azzeer, A. M.; Kienberger, R.; Krausz, F.; Zheltikov, A. M.; Goulielmakis, E. Route to
 Attosecond Nonlinear Spectroscopy. *Phys. Rev. Lett.* **2010**, *105*, 243902.
- 648 (66) Krebs, N.; Pugliesi, I.; Riedle, E. Pulse Compression of Ultrashort UV Pulses by Self-649 Phase Modulation in Bulk Material. *Applied Sciences* **2013**, *3*, 153–167.
- 650 (67) Kobayashi, T.; Kida, Y. Ultrafast spectroscopy with sub-10 fs deep-ultraviolet pulses.

 651 Phys. Chem. Chem. Phys. **2012**, 14, 6200–6210.

- (68) von Korff Schmising, C. et al. Generating circularly polarized radiation in the extreme
 ultraviolet spectral range at the free-electron laser FLASH. Rev. Sci. Instrum. 2017,
 88, 053903.
- (69) Löhl, F.; Arsov, V.; Felber, M.; Hacker, K.; Jalmuzna, W.; Lorbeer, B.; Ludwig, F.;
 Matthiesen, K.-H.; Schlarb, H.; Schmidt, B.; Schmüser, P.; Schulz, S.; Szewinski, J.;
 Winter, A.; Zemella, J. Electron Bunch Timing with Femtosecond Precision in a Superconducting Free-Electron Laser. *Phys. Rev. Lett.* 2010, 104, 144801.
- (70) Inhester, L.; Hanasaki, K.; Hao, Y.; Son, S.-K.; Santra, R. X-Ray Multiphoton Ionization Dynamics of a Water Molecule Irradiated by an x-Ray Free-Electron Laser Pulse.
 Phys. Rev. A 2016, 94, 023422.
- (71) Inhester, L.; Li, Z.; Zhu, X.; Medvedev, N.; Wolf, T. J. Spectroscopic Signature of
 Chemical Bond Dissociation Revealed by Calculated Core-Electron Spectra. J. Phys.
 Chem. Lett. 2019, 10, 6536–6544.
- Krishnan, R.; Binkley, J. S.; Seeger, R.; Pople, J. A. Self-consistent molecular orbital
 methods. XX. A basis set for correlated wave functions. J. Chem. Phys. 1980, 72,
 650–654.
- Glukhovtsev, M. N.; Pross, A.; McGrath, M. P.; Radom, L. Extension of Gaussian 2 (G2) Theory to Bromine- and Iodine-containing Molecules: Use of Effective Core
 Potentials. J. Chem. Phys. 1995, 103, 1878–1885.
- 671 (74) Werner, H.-J.; Knowles, P. J.; Knizia, G.; Manby, F. R.; Schütz, M. Molpro: a general-672 purpose quantum chemistry program package. WIREs Comput Mol Sci **2012**, 2, 242– 673 253.
- (75) Hao, Y.; Inhester, L.; Hanasaki, K.; Son, S.-K.; Santra, R. Efficient Electronic Structure
 Calculation for Molecular Ionization Dynamics at High X-Ray Intensity. Struct. Dyn.
 2015, 2, 041707.

- (76) Cutler, J. N.; Bancroft, G. M.; Tan, K. H. Ligand-field Splittings and Core-level
 Linewidths in I 4d Photoelectron Spectra of Iodine Molecules. J. Chem. Phys. 1992,
 97, 7932–7943.
- 680 (77) Stevens, W. J.; Basch, H.; Krauss, M. Compact effective potentials and efficient shared-681 exponent basis sets for the first- and second-row atoms. *The Journal of Chemical* 682 *Physics* **1984**, *81*, 6026–6033.
- 683 (78) Barca, G. M. J. et al. Recent developments in the general atomic and molecular elec-684 tronic structure system. *The Journal of Chemical Physics* **2020**, *152*, 154102.
- 685 (79) Amini, K.; Savelyev, E.; Brauße, F.; Berrah, N.; Bomme, C.; Brouard, M.; Burt, M.;
 686 Christensen, L.; Düsterer, S.; Erk, B., et al. Photodissociation of aligned CH₃I and
 687 C₆H₃F₂I molecules probed with time-resolved Coulomb explosion imaging by site688 selective extreme ultraviolet ionization. Structural Dynamics **2018**, 5, 014301.